Firdaus *et al. Geoscience Letters* (2024) 11:44
https://doi.org/10.1186/s40562-024-00359-1

Geoscience Letters

RESEARCH LETTER

Open Access

Mechanism of initiation and regeneration of convective cell in Bandung Basin, Indonesia

Irfans Maulana Firdaus[1*], Nurjanna Joko Trilaksono[2] and Takeshi Yamazaki[1]

Abstract

The mechanism of convective cell initiation and regeneration in the Bandung Basin (107.35°E — 107.95°E; 6.75°S — 7.25°S), Indonesia, is investigated using a Weather Research and Forecasting model. Based on the Cumulative Distribution Function and Regeneration Index, model simulations were conducted using case studies in February–March 2019. Upslope wind flows to the mountain peak in north and south of the basin due to solar heating, carrying water vapor from the bottom of the basin. Therefore, low-level convergence is formed due to the convergence of winds from the bottom of the basin and from outside the basin. The low-level convergence causes the developing updraft, makes atmosphere unstable, and generates convective initiation. The convective system will be developed in the mountains region, produced precipitation, and formed cold pools on the surface. The cold pool will fall down the slopes and convective activity from the mountains will continue to the bottom of the basin. The convective system's outflow causes the cold pool to move in the west–east direction. The cold pool will collide with warmer air from the opposite direction, resulting in an updraft at the cold pool leading edge, and convection will be re-initiated (convective regeneration) in the Bandung Basin, with the new convective system tending to move eastward.

Keywords Initiation, Regeneration, Convective cell, Bandung Basin, Cold pool

Introduction

Topography and terrain geometry play an important role in convective initiation, precipitation, and convective regeneration (Jiang 2006; Houze 2012; Watson and Lane 2012; Smith et al. 2015; Kuo and Wu 2019). A concave-shape topography produces more precipitation rather than straight-shape and convex-shape topography (Watson and Lane 2012) because of the confluence zone in the vertex, making upslope ascent stronger, and producing more precipitation (Jiang 2006; Rotunno and Ferretti 2001). Cheng and Yu (2019) have explored the orographic precipitation over a concave-shape topography in Da-Tun Mountain, Taiwan and showed that maximum rainfall is caused by the upslope lifting mechanism. A flow splitting due to mountain blocking from mountain ridges can produce strong convergence between the ridges and cause lifting, making enhanced precipitation (Yu et al. 2022).

In addition to topographic shape, wind patterns can also affect convective initiation (CI) and convective regeneration. Kuo and Wu (2019) have been investigated the mechanisms of CI and regeneration through the ideal case in the Taipei basin and showed that the cold pool plays a role in convective regeneration. Low-level winds passing through the topography in parallel cause the CI, growing into a mature convective system, then generating a cold pool that can cause to regenerate new convective cell (Soderholm et al. 2014; Jeong et al. 2016; Yulihastin et al. 2021).

Mountainous area with the height of more than 2000 m in the north, south, and east part of the Bandung Basin in West Java, Indonesia

*Correspondence:
Irfans Maulana Firdaus
firdaus.irfans.maulana.q6@dc.tohoku.ac.jp
[1] Graduate School of Science, Tohoku University, Sendai, Japan
[2] Atmospheric Sciences Research Group, Faculty of Earth Sciences and Technology, Institut Teknologi Bandung, Bandung, Indonesia

(107.35°E − 107.95°E; 6.75°S − 7.25°S) makes concave-shape topography with the lowest height is around 650 m. Flooding occurs in this lowest height topography frequently, despite the height. Flooding is a disaster that occurs frequently throughout the year. According to BNPB RI (2021), there were 328 (32.06%) floods out of 963 recorded disasters in the Bandung Basin from 2010 to 2021. A long-duration flood occurred in the South Bandung from February to March 2019 and caused material losses and casualties.

Local convective activity influences the precipitation in the Bandung Basin (Dewi and Trilaksono 2018; Fitriani et al. 2019; Oigawa et al. 2017), which can be caused by anabatic and katabatic winds (Kombara et al. 2019). The northern convective system produces earlier precipitation rather than the southern convective system (Dewi and Trilaksono 2018). The CI initiates in the north Bandung Basin and the convective system will propagate to the south, causing convective regeneration (Fitriani et al. 2019). However, Oigawa et al. (2017) conducted simulation in West Java and show that convective activity occurred as a result of reduced static stability due to moisture transport from the bottom of the basin to the south mountains. The convective system propagates to the northern region of West Java, which is different from Fitriani et al. (2019) regarding the location of CI in the Bandung Basin.

Though the regeneration of convective cells in Bandung Basin has been revealed in the previous studies, there is no explanation about the mechanism of initiation and regeneration convective in Bandung Basin. Also, the impact of the topography surrounding Bandung Basin on the initiation and precipitation has been limited. Hence, this study aims to investigate the initiation and possible regeneration mechanism of convective cells in Bandung Basin and examine the impact of topography on the CI.

The remainder of this paper is organized as follows. "Case overview" section provides case selection method from observation data. "Numerical simulation" section describes the numerical model used in this study. "Result and discussion" section provides a detailed mechanism of convective initiation-regeneration and the effect of topography on CI and precipitation. "Summary" section presents a summary of our findings.

Case overview

Balai Besar Wilayah Sungai (BBWS) Citarum is part of the Ministry of Public Works and Public Housing of the Republic of Indonesia, which provides the rainfall observation data in Bandung Basin. To investigate the rainfall characteristics, we use ten precipitation rain gauges data from BBWS Citarum with time interval observation of 10 min during the period 1 February to 31 March 2019. We categorize the regeneration and non-regeneration cases based on Cumulative Distribution Function (CDF) with an upper 20% threshold (P80) and Regeneration Index (RegI). We calculate the P80 for each rain gauge and calculate the mean and median of all rain gauges. The mean and median are used as thresholds and conditions for selecting regeneration and non-regeneration cases based on Eq. 1:

$$\overline{\mathrm{Pr}}_{\mathrm{daily}} \geq \overline{\mathrm{Pr}}_{\mathrm{P80}} \text{ and/or } \mathrm{Pr}_{\mathrm{median}} \geq \mathrm{Pr}_{\mathrm{median\_P80}}, \quad (1)$$

where $\overline{\mathrm{Pr}}_{\mathrm{daily}}$ is daily mean precipitation, $\overline{\mathrm{Pr}}_{\mathrm{P80}}$ is mean precipitation of P80, $\mathrm{Pr}_{\mathrm{median}}$ is median precipitation, and $\mathrm{Pr}_{\mathrm{median\_P80}}$ is median precipitation of P80. There are eight cases that fulfill the conditions (Table 1). To determine the regeneration and non-regeneration cases, we calculate the RegI (Fitriani et al. 2019) for eight cases that pass the condition (Eq. 1). The RegI is given by Eq. 2:

$$\mathrm{RegI} = \frac{\sum \text{Rain Gauge}_{\mathrm{peak}\geq 2}}{\sum \text{Rain Gauge}_{\mathrm{peak}=1}} \quad (2)$$

$\text{Rain Gauge}_{\mathrm{peak}\geq 2}$ is rain gauges that has two or more peak in a day, $\text{Rain Gauge}_{\mathrm{peak}=1}$ is rain gauges that has one peak in a day. We calculate the ratio between the number of stations that has two or more than two peaks in a day and the number of stations which has only one peak in a day for every day for a 2-month period. Table 1 shows the RegI for each case.

The regeneration cases must have RegI > 1. When RegI > 1, the number of stations which have two or more than two peaks in a day is bigger than the number of stations which have one peak in a day. The RegI = 0 indicates that all rain gauges have one peak of rainfall on that day, while 0 < RegI ≤ 1 indicates that the number of stations which have one peak in a day is bigger than the number of stations which have two or more than two peaks in a day. There are two cases, 23 February 2019 and 26 March 2019, that have RegI > 1. However, we only

Table 1 Date and Regeneration Index (RegI) value for eight cases which pass the condition based on Eq. 1

No	Date	RegI
1	03 February 2019	0.13
2	10 February 2019	0.00
3	21 February 2019	0.50
4	23 February 2019	1.67
5	05 March 2019	0.50
6	06 March 2019	0.80
7	26 March 2019	2.33
8	27 March 2019	0.14

use 26 March 2019 to investigate the mechanism initiation and regeneration convective cell in Bandung Basin because it has the highest RegI and the rain gauge, which has two or more than two peaks in a day, is more distributed than other cases (Additional file, Fig. 1).

Numerical simulation

Heavy rainfall occurred in the Bandung area on 26 March 2019, caused flooding in the southern part of Bandung, and 37,731 people were impacted (Cyber, 2019). One of the rain gauges recorded the total precipitation was 83 mm, with a maximum precipitation intensity of 34 mm/h. To simulate the mechanism of initiation and regeneration convective, we perform the convection-permitting simulations using the Advanced Research Weather Research and Forecasting Model (WRF-ARW) model version 4.3.3 (Skamarock et al. 2021) on 26 March 2019. Figure 1 shows the three nested domains with horizontal grid spacings of 9, 3, and 1 km denoted by d01, d02, and d03, respectively. The model simulation runs from 0000 UTC 25 March 2019 and uses NCEP GDAS Final Analysis data (National Centers for Environmental Prediction, National Weather Service, NOAA, U.S. Department of Commerce 2015) with lateral boundary condition updates every 6 h. We also perform the sensitivity parameterization for three physics parameterizations such as microphysics, planetary boundary layer (PBL), and land surface before analyzing the initiation and regeneration mechanism on 26 March 2019 because these three physics parameterizations influence the timing and location of convective initiation (Adams-Selin et al. 2013; Singh et al. 2018). The result of sensitivity parameterization is shown in Additional file 1: Table 1 and Table 2. The configuration parameterization that was used in this present study includes the Betts–Miller–Janjic cumulus scheme (Janjić 1994) for d01, but it was not used in d02 and d03. The three domains use WRF single-moment 3-class (WSM3; Hong et al. 2004) microphysics scheme, Asymmetric Convection Model 2 PBL scheme (ACM2; Pleim 2007), Noah–MP Land Surface scheme

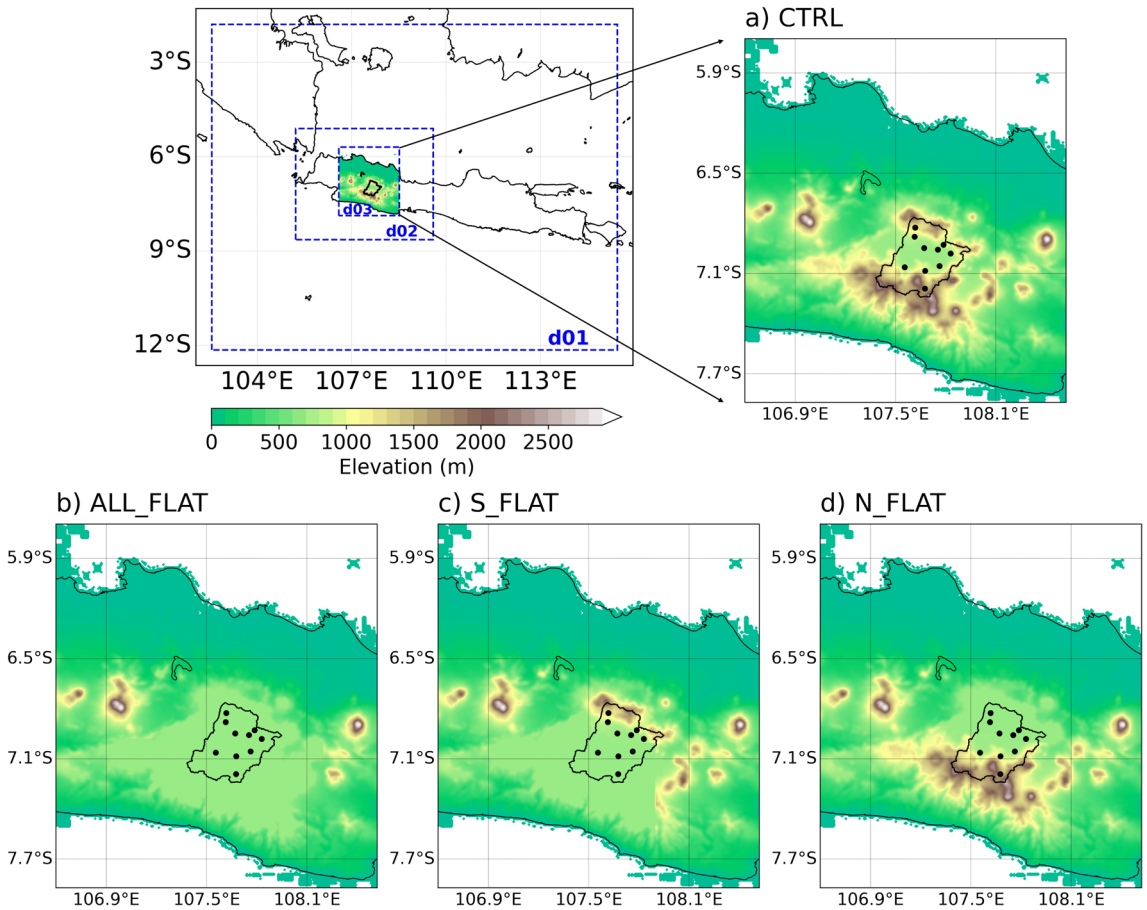

Fig. 1 Model domain with elevation (unit: meter), a black line indicates the Bandung Basin boundaries as control run (CTRL), text d01, d02, and d03 denote the domain 1 (9 km), domain 2 (3 km), and domain 3 (1 km), respectively. **a** CTRL run, the black dot denotes the location of BBWS rain gauges. **b** ALL_FLAT, **c** S_FLAT, and **d** N_FLAT are the experiment runs in "Result and discussion" section

(Noah-MP; Niu et al. 2011), Dudhia shortwave radiation scheme (Dudhia 1989), Rapid and accurate Radiative Transfer Model (RRTM) longwave radiation scheme (Mlawer et al. 1997), and Revised MM5 Monin–Obukhov surface layer scheme (Jiménez et al. 2012).

To investigate the impact of topography surrounding Bandung Basin to the CI, we designed and conducted three experiments in this study as shown in Fig. 1b–d. The ALL_FLAT experiment run removes all mountains surrounding the Bandung Basin (Fig. 1b) to the same height as the lowest height inside the Bandung Basin boundaries (~650 m). Similar to ALL_FLAT, S_FLAT experiment run removes only the southern mountain (Fig. 1c), while N_FLAT experiment run removes only the northern mountain (Fig. 1d). Herein, it is hypothesized that the mechanism of CI is sensitive to the presence of mountains in the north and south Bandung Basin.

Result and discussion

Convective initiation

The convective initiation (CI) is defined as in Abulikemu et al. 2020; Du et al. 2020. To illustrate CI and convective activity in Bandung Basin in detail, Fig. 2 shows the hourly cloud evolution of Himawari 8 satellite composite true color (Akihiro 2020) from 0800 Local Time (LT; UTC+7) to 1000 LT and the hourly evolution of model maximum reflectivity from 0900 to 1400 LT. We use Himawari 8 satellite composite true color (Band 1: 0.47μ, Band 2: 0.51μ, and Band 3: 0.64μ) to validate the convective activity surrounding Bandung Basin because of the absence of radar observation in Bandung Basin. The nearest radar observation is in Tangerang, which is 130–160 km from the Bandung Basin and the range of radar is blocked by topography.

The CI first appeared in the southern mountain of Bandung Basin at 0900 LT (Fig. 2d). It is also confirmed from Himawari 8 satellite composite true color that there is convective activity in the location of CI, which is denoted by white color (Fig. 2a) at 0800 LT. The low-level convergence is formed in the location of CI, denoted by the blue contour (Fig. 2d). The wind surface flows to the southern mountain of the Bandung Basin. This flow merges with the wind that flows from outside Bandung Basin, producing the low-level convergence at the peak of the mountain. Because of radiation heating, the wind flows stronger and makes the convective activity at the peak mountain stronger, both in the southern mountain and the northern mountain. Note that a 1-h time difference between the Himawari 8 satellite composite true color (Fig. 2a–c) and model (Fig. 2d–i). The initiation time errors between model and observation, possibly because of the initial model condition and physics scheme, significantly affect the convective activity (Du et al. 2020) in West Java. Predicting the timing of CI in a complex topography such as West Java is difficult to accomplish, as pointed out by Kain et al. (2013). Regardless of the time difference between the model and observation, the model can capture the features of CI and convective activity in the Bandung Basin and its surroundings.

To further analyze the radiation heating effect on the wind flow, we examined the simulated shortwave radiation in eight locations that is shown in Fig. 3 from 0700 LT until 1200 LT. The shortwave radiation is increasing from 0700 LT until 1200 LT (Additional file, Table 3). It means that the near surface is continually heated and it will affect the temperature. Then, we examined the meridional wind and potential temperature at eight locations for 0700 LT and 1000 LT (Fig. 3). We pair two locations of each valley side of the mountain: location 1^H (higher place than 1^B) and 1^B (lower place than 1^H) in the north mountain valley of the outer basin, location 2^H (higher place than 2^B) and 2^B (lower place than 2^H) in the north mountain valley of the inner basin, location 3^H (higher place than 3^B) and 3^B (lower place than 3^H) in the south mountain valley of the inner basin, and location 4^H (higher place than 4^B) and 4^B (lower place than 4^H) in the south mountain valley of the outer basin to calculate the differences of potential temperature. It shows that the different potential temperature for all pairs is positive, which means that the higher location has a higher potential temperature or warmer than the lower location. The wind speed increases and shows the reverse pattern in the near surface. Wind flows down to the valley (downslope) and has small wind speed at 0700 LT, then flows up to the valley (upslope) and has strong wind speed. The reason for reversing and enhancing wind are the different temperatures along the valley. It produces horizontal pressure gradient force from lower location to higher location during daytime, and is called thermally driven wind (Markowski and Richardson 2010; Chow et al. 2013).

The convective cell that mostly initiates at the peak mountain will merge with another convective cell in the mountain region. These make convective line activity along the mountain (Fig. 2e–i). As shown in Fig. 2g, CI also initiates in the foothills of the northern mountain because of the convergence between gap wind from the west and gap wind from the east. This convective cell merges with the convective system that developed in the northern mountains. The convective system in the northern mountains is earlier mature and dissipates rather than the convective system that developed in the southern mountains. A possible reason is the convergence, which continuously remains in the southern mountain because of flow from the bottom boundary domain and both west

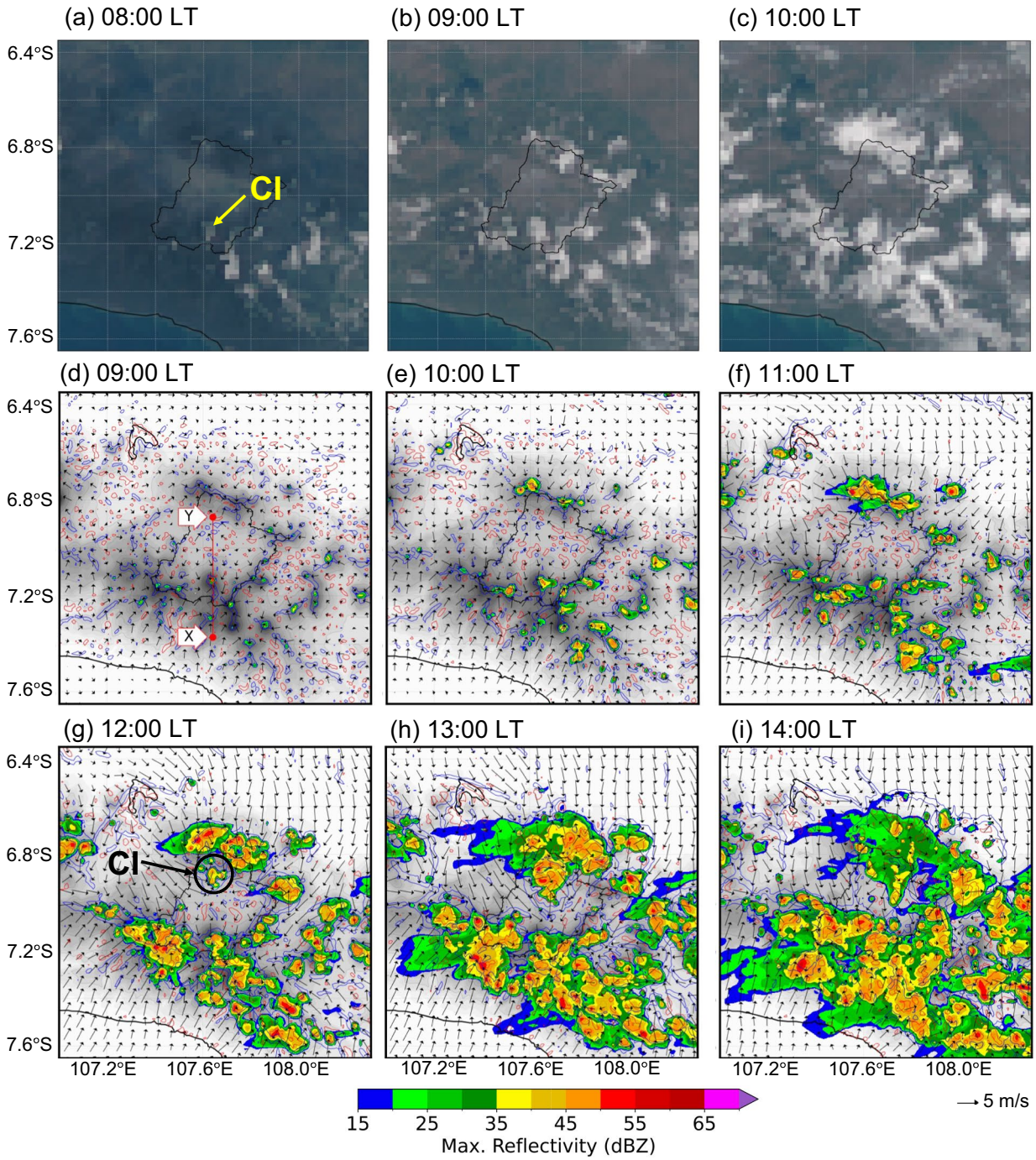

Fig. 2 **a**–**c** Himawari 8 composite true color from 0800 to 1000 LT 26 March 2019. **d**–**i** Hourly Maximum reflectivity (shaded, unit: *dBZ*), surface wind from the bottom of the model (25-m, vector), divergence (red contour, $1 \times 10^{-3} s^{-1}$), convergence (blue contour, $-1 \times 10^{-3} s^{-1}$), black line indicates the Bandung Basin boundaries from 0900 to 1400 LT 26 March 2019. X and Y lines are used to analyze the cross-section in Fig. 3. CI means convective initiation

and east gap winds. The northern mountain convective system propagates to the south and east. Meanwhile, the southern mountain convective system propagates slightly to the north.

Figure 4 shows the cross-section of the CI mechanism associated with low-level convergence along the line XY in Fig. 2d. As shown in Fig. 4a, surface wind from the bottom basin flows to the southern mountain 40 min

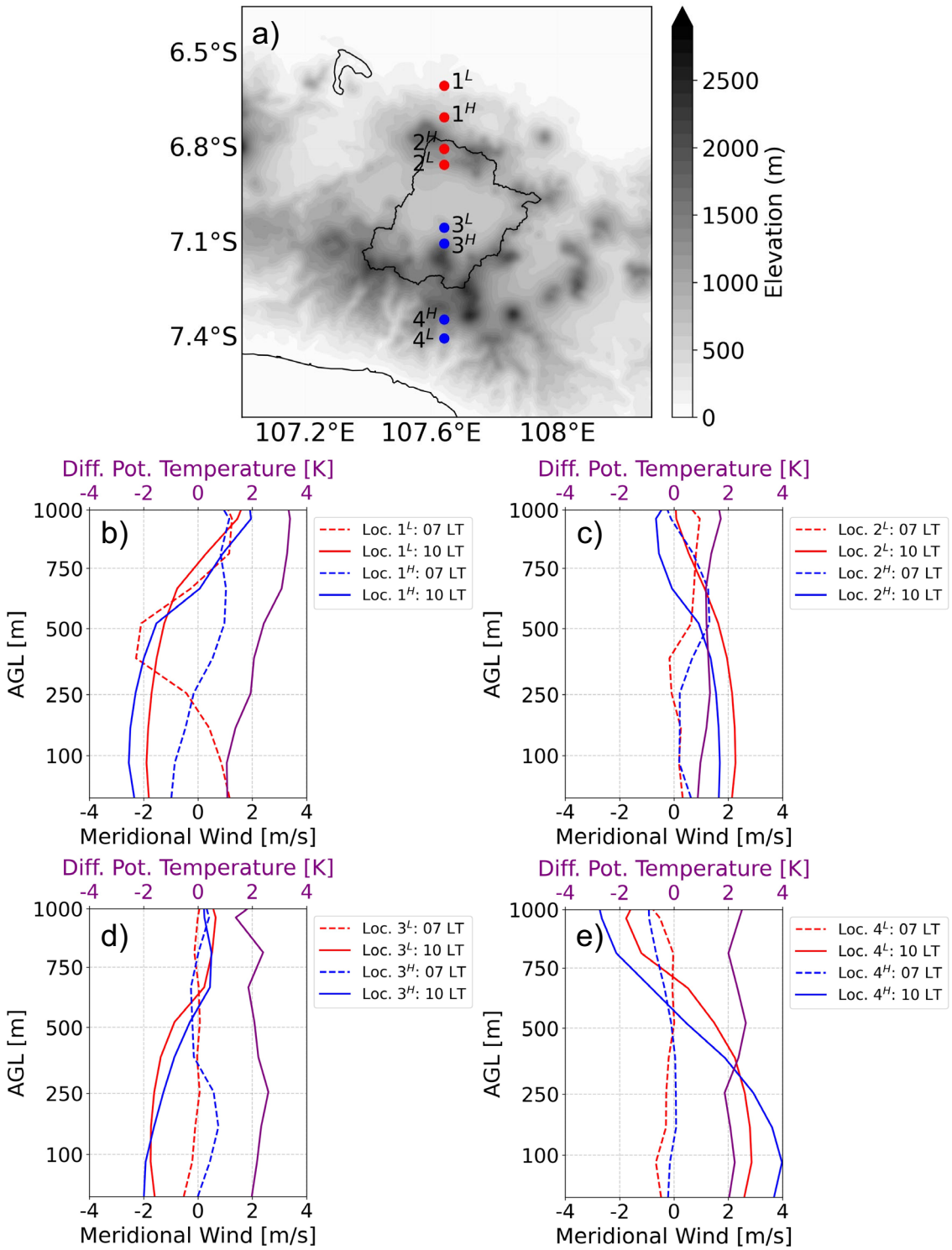

Fig. 3 **a** Eight locations (four pairs) for radiation heating analysis, superscript denoted by H and L mean higher place and lower place. **b**–**e** Meridional temperature (red and blue, unit: *m*/*s*) and different potential temperature (purple, unit: *K*) for 0700 LT and 1000 LT. The different potential temperatures are calculated by subtracting the potential temperature of the higher place and the potential temperature of the lower place

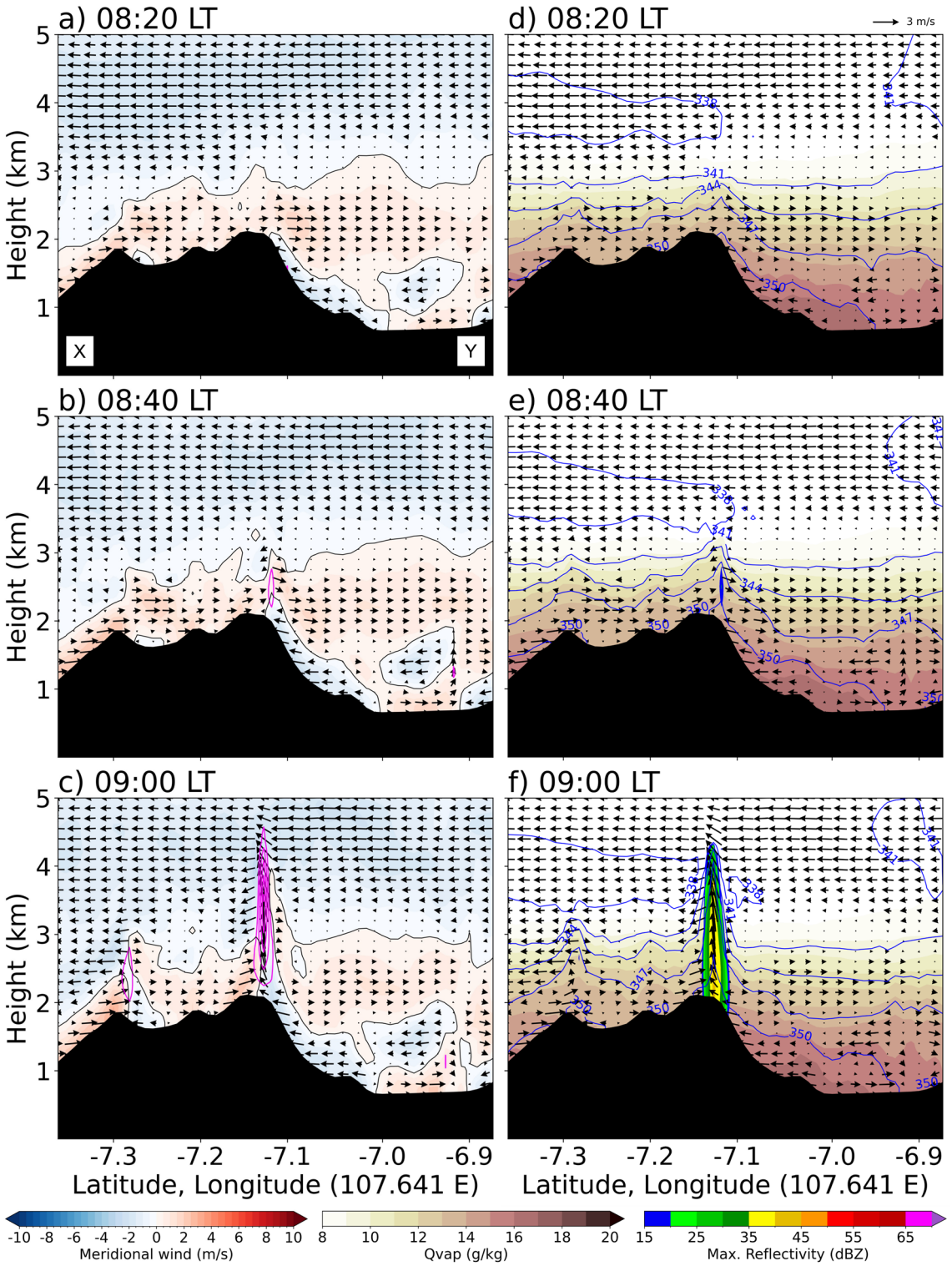

Fig. 4 Vertical cross-section of meridional wind (vector and shaded (positive/red: to the north, negative/blue: to the south), unit: *m*/*s*). **a**–**c** Vertical wind (magenta line from 1 m/s increase per 1 m/s) and black contour indicate meridional wind 0 m/s from 0820 to 0900 LT. **d**–**f** Reflectivity (shaded, unit: *dBZ*), water vapor mixing ratio (*Qv*, shaded, unit: *g*/*kg*), wind (vector, unit: *m*/*s*), and equivalent potential temperature (blue contour, unit: *K*)

(0820 LT) before the time initiation (0900 LT). The wind also carried out water vapor from the bottom basin to the mountain peak (Fig. 4d). The wind from the bottom basin merges with the wind from the outside basin, creating an updraft that is denoted by the magenta line at the mountain peak (Fig. 4b, d). As radiation heated stronger, the updraft also became stronger, causing the atmosphere to become unstable and resulting in the CI at the mountain peak.

To further analyze the source water vapor, we modified the net moisture budget by Du et al. (2020), which is expressed by Eqs. 3, 4, and 5:

$$Q = \frac{1}{g}\int_{h_1}^{h_2} qV\, dh, \tag{3}$$

$$\overline{Q_{x_1x_2}} = \int_{x_1}^{x_2} Q dx, \tag{4}$$

$$Q_{net} = \overline{Q_{south\_plane}} + \overline{Q_{north\_plane}} + \overline{Q_{west\_plane}} + \overline{Q_{east\_plane}}, \tag{5}$$

where g is the gravitational constant, h_1 and h_2 are height of above ground level (0–500 m), $\overline{Q_{x_1x_2}}$ is the plane integration along the boundary from x_1 until x_2. We calculated the net moisture budget around the north and south mountains from 0700 LT until 1000 LT. There are abundant moisture flows to the peak mountains both from the bottom basin and the outer basin (Additional file, Fig. 2).

The impact of topography on convection initiation

To investigate the impact of topography surrounding Bandung Basin on the CI, we conducted the three modifying topography experiments. Figure 5 shows the impact of topography surrounding Bandung Basin on CI. As shown in Fig. 5a–c for ALL_FLAT run, there is no convective activity, which is denoted by maximum reflectivity ≥ 35 dBZ in the southern Bandung Basin, especially in the location of CI CTRL run (Fig. 2a). The low-level convergence forms in the southern West Java at 1000 LT (Fig. 5b) and in the northern West Java at 1100 LT (Fig. 5c), because the wind from bottom boundaries domain merges with the wind from top of flat topography. In contrast with ALL_FLAT run, S_FLAT run and N_FLAT run show convective activity on the mountain peak (Fig. 5d–i). The CI in the N_FLAT run is delayed, compared to the result of the CTRL run around 20 min. Nevertheless, the convective activity N_FLAT run (Fig. 5d–f) in the southern mountain is quite similar with CTRL run (Fig. 2a–c). The convective cells merge with another convective cell along the topography. In contrast to the N_FLAT run, the S_FLAT run shows that the CI delay is around 10 min, compared to the CTRL run, in the northern mountain and there is no convective activity in the southern Bandung Basin because of the absence of the southern mountain (Fig. 5g–i).

The simulation of modified topography results indicates that topography in the southern and northern Bandung Basin greatly influence the CI. This result is consistent with the previous study results (e.g., Chen et al. 2011, 2013; Du et al. 2020; Li et al. 2021) for the topography effect on the convective activity. The absence of southern and northern topography in the Bandung Basin causes the lack of low-level convergence and is inadequate to trigger the CI due to decrease of moisture flux. This result also similar with Rasmussen and Houze (2016), who have explored the effect of the Andes, South America on the CI and showed that removing 50% topography will decrease the moisture flux convergence and less convection.

Convective regeneration

The definition of convective regeneration is that a new convective cell appears (cell t + 1) after the previous convective cell (cell t) produces precipitation and dissipates (weakening). Convective regeneration can occur in a similar place as the predecessor convective cell or in another place. This present study hypothesizes that convective cell initiates in certain locations, grow into convective system, and produce precipitation. The precipitation generates the formation of a cold pool, which triggers the regeneration of convective cells. The identification of a cold pool uses potential temperature (θ) and buoyancy (b) at the lowest level of the model (~25 m). Buoyancy is a quantity used to examine the cold pools (Hirt et al. 2020; Tompkins 2001). The buoyancy equation is given by Eqs. 6 and 7:

$$b = \frac{g\left(\theta_\rho - \overline{\theta_\rho}\right)}{\overline{\theta_\rho}}, \tag{6}$$

$$\theta_\rho = \theta\left(1 + 0.608q_v - q_c - q_r - q_i - q_g - q_s\right), \tag{7}$$

where b is buoyancy (m/s^2), g is gravitation (m/s^2), θ_ρ is temperature density (K), $\overline{\theta_\rho}$ is horizontal mean temperature density (K), and $q_v, q_c, q_r, q_i, q_g, q_s$ is mixing ratio for water vapor, cloud, rain, ice, graupel, and snow, respectively. To identify the cold pool boundaries, we follow the threshold value $b \leq -0.005\ m/s^2$ from Tompkins (2001) because it can capture the cold pools that coincide with the precipitation region.

As explained in the previous section, the northern mountain convective system propagates to the south and it coincides with the propagating cold pool to the south (Fig. 6a–d). The convective system produces the

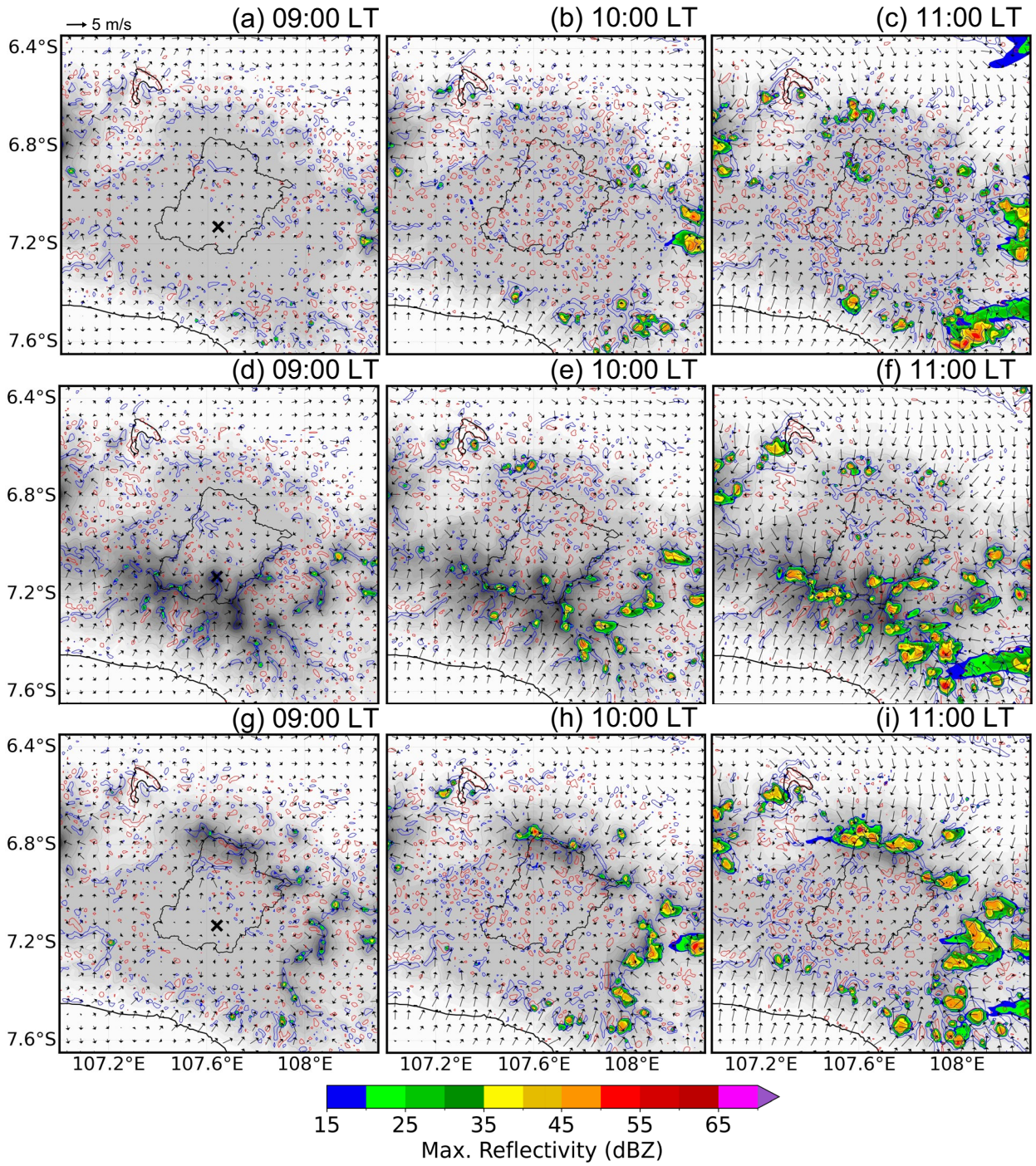

Fig. 5 Same as Fig. 2a–c, but for three experiment runs. **a**–**c** ALL_FLAT, **d**–**f** N_FLAT, and **g**–**i** S_FLAT from 0900 to 1100 LT 26 March 2019. The black mark 'X' denotes the location of CI based on the CTRL experiment run

precipitation in the northern mountain, resulting in surface air becoming cool. This cold pool falls down through the valley and reaches the bottom basin. Meanwhile, the cold pool that is generated in the southern mountain propagates slightly to the north due to the gap wind from the west that prevents the southern convective system from propagating further. Cold pool that reach the bottom basin tend to propagate to the east because of strong wind from the west (Fig. 2h, i).

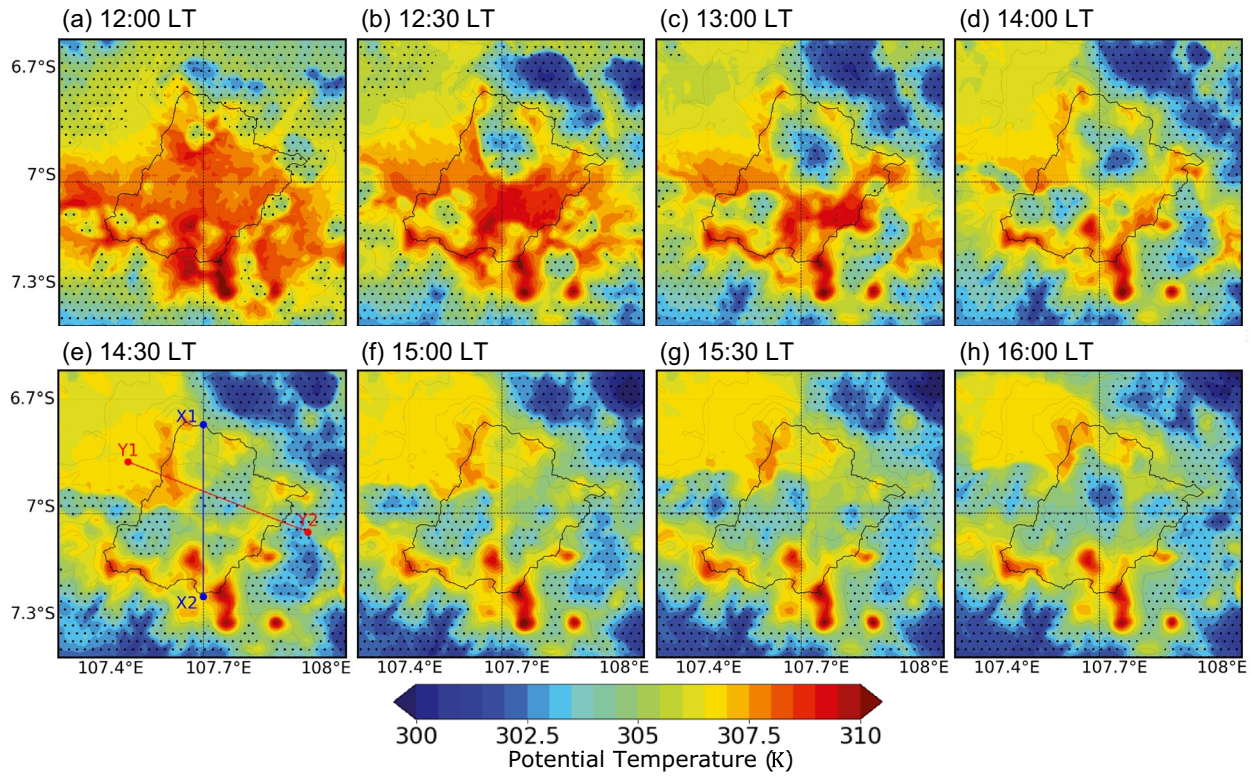

Fig. 6 **a**–**h** Potential temperature (shaded: *K*), and buoyancy (black dot, $b \leq -0.005 m/s^2$) from 1200 to 1600 LT 26 March 2023. The X1-X2 and Y1-Y2 in **e** 1430 LT are used to analyze the vertical cross-section in Figure

Figures 7 and 8 show the detail of cold pool propagation and convective regeneration. Figure 7a–c shows convective cell initiates in the foothill of the northern mountain denoted by CS1 (Convective System 1), as pointed out in the previous section. The CS1 grows and merges with the northern mountain convective system (Fig. 7d–f), producing precipitation. The cold pool that exists in the northern mountain falls down to the valley and reaches the center of the basin (Fig. 7g–r). The CS1 continues to propagate to the east because of strong wind from the west, as shown in Fig. 8 from 1330 to 1500 LT and starts to dissipate at 1400 LT. This pattern also appeared on 23 February 2019. The cold pool exists in the southern mountain, falls down to the valley, and reaches the center of the basin.

The new convective cell initiates inside the basin, denoted by CS2 in Fig. 8 at 1440 LT (also shown in Additional file: Fig. 3 denoted by CR). The CS1 produces precipitation and subsequent evaporation creates a downdraft. The downdraft spreads as it reaches the surface, as shown in Fig. 8 at 1330 LT, as pointed out by Markowski and Richardson (2010). It spreads westward and eastward, pushing the cold pool to the west and east of the Bandung Basin. The cold pool collides with warm air from west, making a new convective cell as denoted by CS2 at 1440 LT. The CS2 develops and propagates tend to eastward. It is shown that the cold pool indeed exerts an important factor in the convective regeneration in Bandung Basin.

Summary

In the current study, we investigate the mechanism of convective initiation and regeneration in Bandung Basin, Indonesia, using the WRF model. A rainfall event on 26 March 2019 was used as the case study based on the Cumulative Distribution Function (CDF) and Regeneration Index (RegI) calculation. A convection-permitting WRF-ARW simulation with a horizontal grid spacing of 1 km can capture the location of CI compared to those of the observations. The wind flow from the bottom basin carrying water vapor merges with the wind flow from the outside of the basin at the mountain peak. These winds create a low-level convergence in the mountain peak region. The low-level convergence reinforces the updraft, makes the atmosphere unstable, and forms the CI.

By carrying out the modified topography experiments, we attempt to clarify the role of southern and northern mountains in the Bandung Basin to the CI. When the northern and southern mountains are removed, there is no convective activity in both regions due to the absence

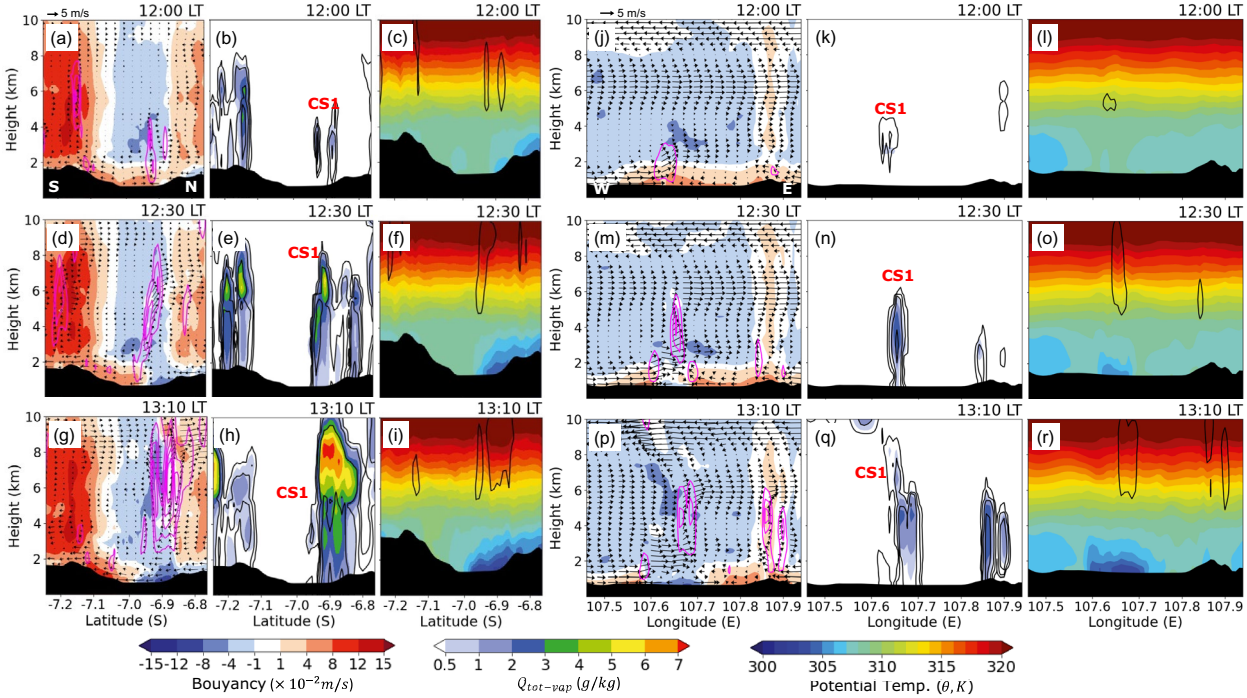

Fig. 7 Vertical cross-section of **a**–**i** X1-X2 and **j**–**r** Y1-Y2 from Fig. 5e. The first (**a**, **d**, **g**) and fourth (**j**, **m**, **p**) column panel are buoyancy (shaded), vertical wind (magenta contour with interval 1 *m*/*s*), meridional wind (first column panel), and zonal wind (fourth column panel) (vector, *m*/*s*). The second (**b**, **e**, **h**) and fifth (**k**, **n**, **q**) column panel are total mixing ratio except water vapor mixing ratio (shaded) and reflectivity (black contour from 15 *dBZ* with interval 10 *dBZ*). The third (**c**, **f**, **i**) and sixth (**l**, **o**, **r**) column panel are potential temperature (shaded) and cloud mixing ratio (contour, 0.5 *g*/*kg*). CS1 indicates the Convective System 1

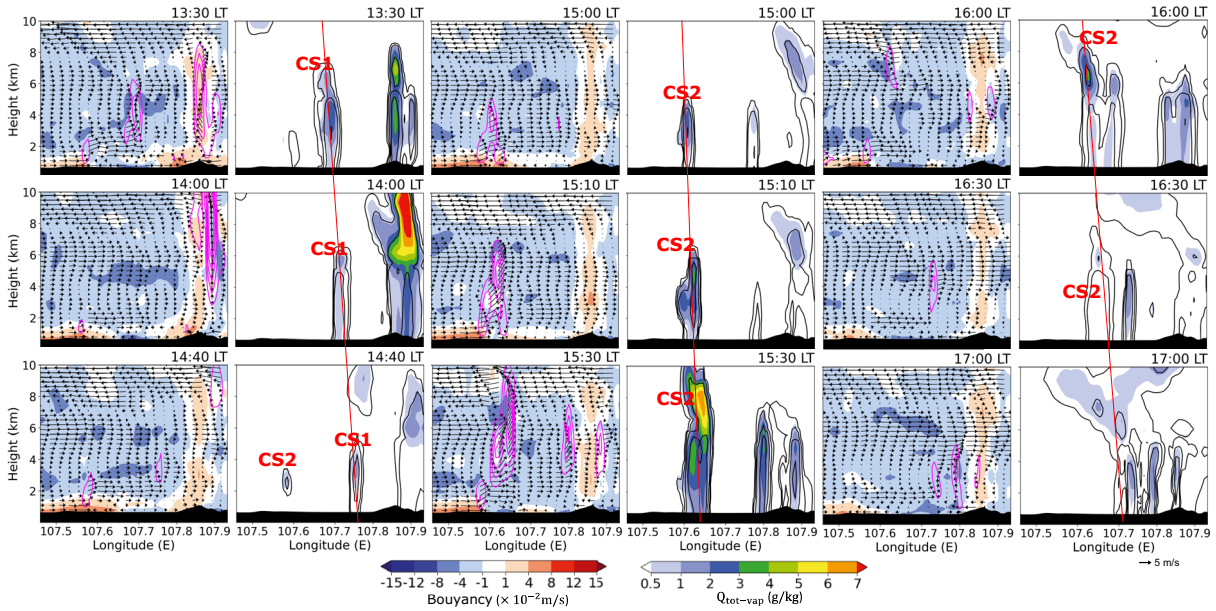

Fig. 8 The first, third, and fifth column panel are buoyancy (shaded), vertical wind (magenta contour with interval 1 *m*/*s*), and zonal wind (vector, *m*/*s*). The second, fourth, and sixth column panel are total mixing ratio except water vapor mixing ratio (shaded) and reflectivity (black contour from 15 *dBZ* with interval 10 *dBZ*). CS1 and CS2 indicate Convective System 1 and Convective System 2

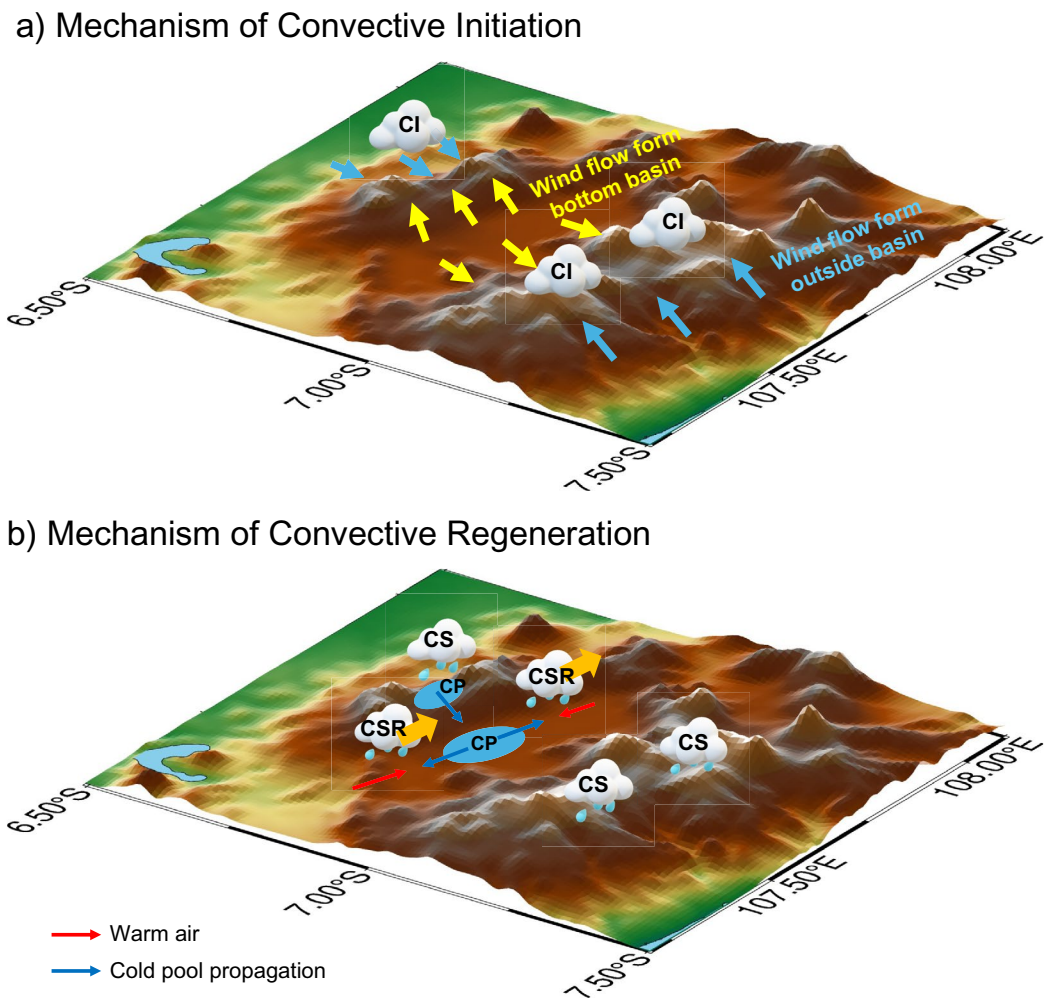

Fig. 9 Schematic diagram mechanism of initiation and regeneration convective in Bandung Basin. CI is convective initiation, CS is convective system, CSR is convective system regeneration, and CP is cold pool

of lifting and low-level convergence. These experiments also revealed that topography influences the CI timing.

The convective system that developed in mountains produces rainfall and generates a cold pool on the surface. The cold pool will fall down to the valley and reaches the center basin. The outflow from the convective system causes the cold pool to spread westward and eastward. The cold pool will collide with warmer air from the opposite direction, resulting in an updraft at the cold pool leading edge (CPLE) and convective will re-initiate (convective regeneration) in the Bandung Basin, with the new convective system tending to move eastward. The process mechanism of the initiation and regeneration convective system in Bandung Basin is summarized in Fig. 9.

The present study gives understanding about the mechanism of CI and convective regeneration in basin area, especially in Bandung Basin, Indonesia. Also, it gives clarity about the role of mountains surrounding Bandung Basin to the CI. The effect of land use and the interaction between sea–land breeze and mountain breeze in the southern mountain were not discussed in the present study, which is important to investigate in the future.

Supplementary Information

The online version contains supplementary material available at https://doi.org/10.1186/s40562-024-00359-1.

Additional file 1.

Acknowledgements

The first author was funded by a scholarship from Japan International Cooperation Agency (JICA) under Human Resources Development in Science, Technology and Innovation Program. The first author would like to thank Indonesian Endowment Fund (LPDP Republik Indonesia) for the support. This work is supported by MEXT-Program for the Advanced Studies of Climate Change Projection (SENTAN) Grant Number JPMXD0722680734. This work used the supercomputing resources provided by the Cyberscience Center, Tohoku

University, Japan. The authors gratefully acknowledge the BBWS Citarum for the rain gauges precipitation data (http://103.184.53.146/).

Author contributions
IMF conducted the data processing, analysis, visualization, and writing the manuscript. NJT provided helpful insight in the analysis, editorial aspects, and revised the manuscript. TY is providing insight in additional experiments and editorial aspects. All authors read and approved the final manuscript.

Funding
This research is funded by the Japan International Cooperation Agency (JICA) under Human Resources Development in Science, Technology and Innovation Program, and MEXT-Program for the Advanced Studies of Climate Change Projection (SENTAN) Grant Number JPMXD0722680734.

Availability of data and materials
The datasets generated and/or analyzed in this study are available upon request from the corresponding author on reasonable request.

Declarations

Competing interests
The authors declare that they have no competing interests.

Received: 6 March 2024 Accepted: 19 September 2024
Published online: 30 September 2024

References

Abulikemu A, Ming J, Xu X, Zhuge X, Wang Y, Zhang Y, Zhang S, Yu B, Aireti M (2020) Mechanisms of convection initiation in the Southwestern Xinjiang, Northwest China: a case study. Atmosphere. https://doi.org/10.3390/atmos11121335

Adams-Selin RD, van den Heever SC, Johnson RH (2013) Sensitivity of bow-echo simulation to microphysical parameterizations. Weather Forecast 28(5):1188–1209. https://doi.org/10.1175/WAF-D-12-00108.1

Akihiro S (2020) Introduction to Himawari-8 RGB composite imagery. Meteorological Satellite Center Technical Note, 65.

BNPB RI (2021) Data bencana - geoportal data bencana indonesia. Accessed online at https://dibi.bnpb.go.id/

Chen C-S, Lin Y-L, Hsu N-N, Liu C-L, Chen C-Y (2011) Orographic effects on localized heavy rainfall events over southwestern Taiwan on 27 and 28 June 2008 during the post-Mei-Yu period. Int Conf Nucleation Atmospheric Aerosols 101(3):595–610. https://doi.org/10.1016/j.atmosres.2011.04.004

Chen C-S, Lin Y-L, Zeng H-T, Chen C-Y, Liu C-L (2013) Orographic effects on heavy rainfall events over northeastern Taiwan during the northeasterly monsoon season. Atmos Res 122:310–335. https://doi.org/10.1016/j.atmosres.2012.10.008

Cheng L-W, Yu C-K (2019) Investigation of orographic precipitation over an isolated, three-dimensional complex topography with a dense gauge network, radar observations, and upslope model. J Atmos Sci 76(11):3387–3409. https://doi.org/10.1175/JAS-D-19-0005.1

Chow FK, De Wekker SFJ, Snyder BJ (2013) Mountain weather research and forecasting. Springer, Dordrecht. https://doi.org/10.1007/978-94-007-4098-3

Dewi ES, Trilaksono NJ (2018) Analysis of localized rainfall by using grid observation data of automatic weather station in Bandung basin case studies 28 February and 9 March 2017. AIP Conf Proc 1987(1):020050. https://doi.org/10.1063/1.5047335

Du Y, Chen G, Han B, Bai L, Li M (2020) Convection initiation and growth at the coast of South China. Part II: effects of the terrain, coastline, and cold pools. Mon Weather Rev 148(9):3871–3892. https://doi.org/10.1175/MWR-D-20-0090.1

Dudhia J (1989) Numerical study of convection observed during the winter monsoon experiment using a mesoscale two-dimensional model. J Atmospheric Sci 46(20):3077–3107. https://doi.org/10.1175/1520-0469(1989)046%3c3077:NSOCOD%3e2.0.CO;2

Fitriani R, Trilaksono NJ, Hadi TW (2019) Investigation of the regeneration of precipitating convective cloud in basin topography area. IOP Conf Ser Earth Environ Sci 303(1):012015. https://doi.org/10.1088/1755-1315/303/1/012015

Hirt M, Craig GC, Schäfer SAK, Savre J, Heinze R (2020) Cold-pool-driven convective initiation: using causal graph analysis to determine what convection-permitting models are missing. Q J R Meteorol Soc 146(730):2205–2227. https://doi.org/10.1002/qj.3788

Hong S-Y, Dudhia J, Chen S-H (2004) A revised approach to ice microphysical processes for the bulk parameterization of clouds and precipitation. Mon Weather Rev 132(1):103–120. https://doi.org/10.1175/1520-0493(2004)132%3c0103:ARATIM%3e2.0.CO;2

Houze RA Jr (2012) Orographic effects on precipitating clouds. Rev Geophys. https://doi.org/10.1029/2011RG000365

Janjić ZI (1994) The step-mountain eta coordinate model: further developments of the convection, viscous sublayer, and turbulence closure schemes. Mon Weather Rev 122(5):927–945. https://doi.org/10.1175/1520-0493(1994)122%3c0927:TSMECM%3e2.0.CO;2

Jeong J-H, Lee D-I, Wang C-C (2016) Impact of the cold pool on mesoscale convective system-produced extreme rainfall over Southeastern South Korea: 7 July 2009. Mon Weather Rev 144(10):3985–4006. https://doi.org/10.1175/MWR-D-16-0131.1

Jiang Q (2006) Precipitation over concave terrain. J Atmos Sci 63(9):2269–2288. https://doi.org/10.1175/JAS3761.1

Jiménez PA, Dudhia J, González-Rouco JF, Navarro J, Montávez JP, García-Bustamante E (2012) A revised scheme for the WRF surface layer formulation. Mon Weather Rev 140(3):898–918. https://doi.org/10.1175/MWR-D-11-00056.1

Kain JS, Coniglio MC, Correia J, Clark AJ, Marsh PT, Ziegler CL, Lakshmanan V, Miller SD, Dembek SR, Weiss SJ, Kong F, Xue M, Sobash RA, Dean AR, Jirak IL, Melick CJ (2013) A feasibility study for probabilistic convection initiation forecasts based on explicit numerical guidance. Bull Am Meteor Soc 94(8):1213–1225. https://doi.org/10.1175/BAMS-D-11-00264.1

Kombara PY, Junnaedhi IDGA, Riawan E (2019) Characteristic of anabatic wind in Bandung basin observed by AWS. IOP Conf Ser Earth Environ Sci 303(1):012010. https://doi.org/10.1088/1755-1315/303/1/012010

Kuo K-T, Wu C-M (2019) The precipitation hotspots of afternoon thunderstorms over the Taipei basin: idealized numerical simulations. J Meteorol Soc Japan 97(2):501–517. https://doi.org/10.2151/jmsj.2019-031

Li H, Huang Y, Hu S, Wu N, Liu X, Xiao H (2021) Roles of terrain, surface roughness, and cold pool outflows in an extreme rainfall event over the coastal region of South China. J Geophys Res Atmospheres 126(23):e2021JD035556. https://doi.org/10.1029/2021JD035556

Markowski P, Richardson Y (2010) Organization of isolated convection. In: Markowski P, Richardson Y (eds) Mesoscale meteorology in midlatitudes. John Wiley & Sons, Ltd., Hoboken, pp 201–244

Mlawer EJ, Taubman SJ, Brown PD, Iacono MJ, Clough SA (1997) Radiative transfer for inhomogeneous atmospheres: RRTM, a validated correlated-k model for the longwave. J Geophys Res Atmospheres 102(D14):16663–16682. https://doi.org/10.1029/97JD00237

Niu G-Y, Yang Z-L, Mitchell KE, Chen F, Ek MB, Barlage M, Kumar A, Manning K, Niyogi D, Rosero E, Tewari M, Xia Y (2011) The community Noah land surface model with multiparameterization options (Noah-MP): 1. Model description and evaluation with local-scale measurements. J Geophys Res 116(D12):D12109. https://doi.org/10.1029/2010JD015139

National Centers for Environmental Prediction, National Weather Service, NOAA, U.S. Department of Commerce (2015) *NCEP GDAS/FNL 0.25 Degree Global Tropospheric Analyses and Forecast Grids*. Research Data Archive at the National Center for Atmospheric Research, Computational and Information Systems Laboratory. https://doi.org/10.5065/D65Q4T4Z

Oigawa M, Matsuda T, Tsuda T, Noersomadi (2017) Coordinated observation and numerical study on a diurnal cycle of tropical convection over a complex topography in West Java, Indonesia. J Meteorol Soc Japan 95(4):261–281. https://doi.org/10.2151/jmsj.2017-015

Pleim JE (2007) A combined local and nonlocal closure model for the atmospheric boundary layer. Part I: model description and testing. J Appl Meteorol Climatol 46(9):1383–1395. https://doi.org/10.1175/JAM2539.1

Rasmussen KL, Houze RA (2016) Convective initiation near the Andes in Subtropical South America. Mon Weather Rev 144(6):2351–2374. https://doi.org/10.1175/MWR-D-15-0058.1

Rotunno R, Ferretti R (2001) Mechanisms of intense alpine rainfall. J Atmos Sci 58(13):1732–1749. https://doi.org/10.1175/1520-0469(2001)058%3c1732:MOIAR%3e2.0.CO;2
Singh KS, Bonthu S, Purvaja R, Robin RS, Kannan BAM, Ramesh R (2018) Prediction of heavy rainfall over Chennai Metropolitan City, Tamil Nadu, India: impact of microphysical parameterization schemes. Atmos Res 202:219–234. https://doi.org/10.1016/j.atmosres.2017.11.028
Skamarock C, Klemp B, Dudhia J, Gill O, Liu Z, Berner J, Wang W, Powers G, Duda G, Barker D, Huang X (2021) A Description of the Advanced Research WRF Model Version 4.3. https://doi.org/10.5065/1dfh-6p97
Smith VH, Mobbs SD, Burton RR, Hobby M, Aoshima F, Wulfmeyer V, Di Girolamo P (2015) The role of orography in the regeneration of convection: a case study from the convective and orographically? Induced precipitation study. Meteorol Z 24(1):83–97. https://doi.org/10.1127/metz/2014/0418
Soderholm B, Ronalds B, Kirshbaum DJ (2014) The evolution of convective storms initiated by an isolated mountain ridge. Mon Weather Rev 142(4):1430–1451. https://doi.org/10.1175/MWR-D-13-00280.1
Tompkins AM (2001) Organization of Tropical convection in low vertical wind shears: the role of cold pools. J Atmos Sci 58(13):1650–1672. https://doi.org/10.1175/1520-0469(2001)058%3c1650:OOTCIL%3e2.0.CO;2
Watson CD, Lane TP (2012) Sensitivities of orographic precipitation to terrain geometry and upstream conditions in idealized simulations. J Atmos Sci 69(4):1208–1231. https://doi.org/10.1175/JAS-D-11-0198.1
Yu C-K, Liu W-F, Cheng L-W, Lin C-Y (2022) Mechanisms of valley precipitation enhancement over Da-Tun mountain. Mon Weather Rev 150(7):1851–1871. https://doi.org/10.1175/MWR-D-21-0195.1
Yulihastin E, Fathrio I, Trismidianto, Nauval F, Saufina E, Harjupa W, Satiadi D, Nuryanto DE (2021) Convective cold pool associated with offshore propagation of convection system over the east coast of Southern Sumatra, Indonesia. Adv Meteorol 2021:2047609. https://doi.org/10.1155/2021/2047609

Publisher's Note